Journal of Materials Chemistry A

ROYAL SOCIETY OF CHEMISTRY

PAPER

View Article Online
View Journal | View Issue

Check for updates

Cite this: *J. Mater. Chem. A*, 2023, **11**, 12214

Harnessing ion–dipole interactions: a simple and effective approach to high-performance lithium receptors†

Chengkai Xu, Quy Tran, Lukasz Wojtas and Wenqi Liu *

Received 27th March 2023
Accepted 22nd May 2023

DOI: 10.1039/d3ta01831h

rsc.li/materials-a

The burgeoning demand for lithium across various sectors, most notably in lithium-ion batteries, necessitates the development of efficient extraction and purification methodologies. As a response to this imperative, the design of synthetic receptors exhibiting high selectivity and affinity for lithium ions has emerged as a crucial area of research. This investigation proposes a simple and effective approach to high-performance lithium receptors that capitalizes on ion–dipole interactions as the principal driving force for lithium binding. Our investigation encompasses the design, synthesis, and evaluation of five distinct ionophores characterized by varied ion–dipole interactions with lithium, culminating in significantly enhanced binding affinity and Li^+/Na^+ selectivity compared to conventional macrocyclic crown ether-based receptors. Moreover, we identify a new building block based on pyridine-*N*-oxide, which serves as an efficacious motif for developing receptors with augmented lithium-binding capacities. Additionally, our findings demonstrate a rapid and efficient solid–liquid extraction process for LiCl in the presence of a substantial excess of NaCl and KCl, employing the newly discovered ionophore. Collectively, this study contributes valuable insights into molecular design strategies for high-performance lithium receptors and advocates for continued exploration of sustainable molecular materials to enhance lithium recognition and extraction efficiencies.

Department of Chemistry, University of South Florida, 4202 E. Fowler Ave, Tampa, FL, 33620, USA. E-mail: wenqi@usf.edu

† Electronic supplementary information (ESI) available. CCDC 2252048. For ESI and crystallographic data in CIF or other electronic format see DOI: https://doi.org/10.1039/d3ta01831h

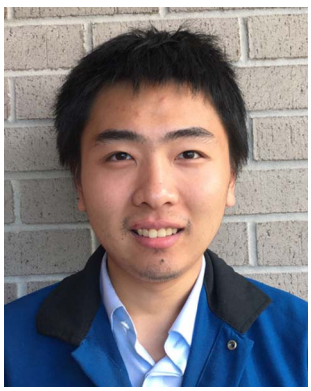

Chengkai Xu is a PhD student in the Department of Chemistry at the University of South Florida. He received his BSc in Chemistry from Zhejiang University in 2020. His research interests lie in the development of molecular receptors for critical minerals and biomolecules.

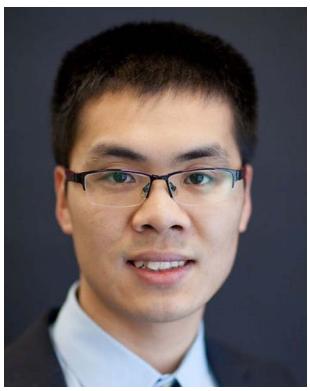

Dr Wenqi Liu is an Assistant Professor in the Department of Chemistry at the University of South Florida. He received his BSc in Chemistry from Shandong University in 2013 and his PhD in Supramolecular Organic Chemistry from the University of Notre Dame in 2018 under the supervision of Professor Bradley Smith. He then conducted post-doctoral research at Northwestern University from 2018 to 2021, working with Professor Fraser Stoddart. Dr Liu's research interests lie in host–guest chemistry, particularly in relation to critical minerals and bioactive molecules. He is interested in designing and synthesizing functional molecular materials to address challenges in clean energy and health.

Introduction

Lithium (Li^+) has emerged as a critical element due to its extensive applications across pharmaceutical, scientific, and technological sectors. As a mood stabilizer, Li^+ serves a crucial role in treating depression and various mental health disorders.[1,2] Moreover, it is utilized to enhance strength and thermal stability in the ceramics and glass industries and improve lubricants' viscosity.[3,4] The most significant application of Li^+ lies in its indispensable role as a key component in lithium-ion batteries.[5–8] The ongoing global energy transition from fossil fuels to renewable sources has precipitated a Li^+ supply crisis, highlighting the imperative to develop novel technologies for extracting and enriching Li^+ from natural resources and anthropogenic waste.[9–15] Consequently, the design and implementation of molecular receptors capable of effectively recognizing, sensing, extracting, and purifying this critical mineral have become paramount in addressing this pressing challenge.[16–22]

The design and synthesis of high-performance receptors for Li^+ have traditionally focused on developing macrocyclic receptors, featuring small binding cavities meticulously tailored[19,20,23–30] to selectively bind Li^+ while excluding competing ions such as sodium (Na^+) and potassium (K^+). A pioneering work in this domain was exemplified[31–36] by Donald Cram's spherands, which displayed an extraordinary binding affinity exceeding 10^{16} M^{-1} for Li^+ due to their rigid and preorganized binding cavities. In alignment with this foundational principle, numerous macrocyclic scaffolds have been devised for Li^+ binding, employing molecular design strategies based on crown ether derivatives,[21,27,28,37–43] ion pair receptors,[16,25,25,44–48] mechanically interlocked molecules,[26,49–52] and organometallic macrocycles.[18,19,29,53] However, despite the success in achieving strong binding affinity for Li^+, the majority of these macrocyclic receptors exhibit limited Li^+/Na^+ selectivity (ratio <1000) and necessitate high-dilution conditions during synthesis. These constraints present considerable challenges for large-scale production and the practical implementation of these receptors in Li^+ extraction and separation processes.

In contrast to macrocyclic receptors, acyclic receptors[54–57] offer a relatively straightforward synthesis process. However, their inherent flexibility complicates the achievement of effective selectivity without relying on size matching. We hypothesize that addressing this challenge is achievable by leveraging[58] the high charge density inherent to Li^+, enabling the establishment of selectivity predicated upon ion–dipole interactions within the context of acyclic receptor architectures. This study introduces a simple and effective approach to high-performance Li^+ receptors, emphasizing ion–dipole interactions as the primary driving force for selective Li^+ binding. Our research encompasses the design, synthesis, and evaluation of five ionophores that display strong ion–dipole interactions with Li^+, resulting in superior binding affinity and Li^+/Na^+ selectivity compared to conventional macrocyclic crown ether-based receptors. Additionally, we uncover a new building block based upon pyridine-*N*-oxide, serving as an effective motif for designing receptors with augmented Li^+ binding capabilities. Our results further illustrate a rapid and efficient solid–liquid extraction process for LiCl in the presence of a substantial excess of NaCl and KCl, employing the newly identified ionophore. This investigation provides valuable insights into molecular design strategies for high-performance Li^+ receptors and paves the way for continued exploration of cutting-edge molecular architectures to achieve sustainable molecular materials with enhanced Li^+ recognition and extraction efficiencies.

Experimental

Synthesis

P1. To a solution of 2,2-dibenzylpropane-1,3-diol (1.95 mmol, 1.0 eq., 500 mg) in dry DMF (15 mL) was added NaH (3.0 eq., 204 mg, 60% in mineral oil) in portions. The mixture was stirred for one hour at room temperature. 2-Bromopyridine (4.88 mmol, 2.5 eq., 77 0 mg) was then added dropwise. When the addition was done, the temperature was raised to 80 °C and stirred overnight. The reaction was quenched with water, poured into ice water (150 mL), and extracted by ethyl acetate (3 × 30 mL). The combined organic phase was washed with water (3 × 30 mL) and brine (2 × 30 mL). The solvent was removed under vacuum, and the residue was purified by flash column chromatography (hexanes/EtOAc) to afford precursor P1 (57%, 460 mg) as a white solid. ^{1}H NMR (400 MHz, $CDCl_3$) δ 8.13 (dd, J = 5.1, 2.0 Hz, 2H), 7.66–7.58 (m, 2H), 7.15 (m, 10H), 6.92–6.82 (m, 4H), 4.01 (s, 4H), 3.05 (s, 4H). ^{13}C NMR (151 MHz, $CDCl_3$) δ 163.7, 147.2, 138.6, 137.5, 130.7, 128.1, 126.2, 116.8, 110.9, 66.0, 42.9, 39.2. HRMS-ESI: calcd for $C_{27}H_{26}N_2O_2$ $[M + H]^+$: 410.1994 found: 410.1999.

I5. To a solution of precursor P1 (200 mg, 0.49 mmol, 1.0 eq.) in $CHCl_3$ (5 mL), *m*-CPBA (1.46 mmol, 3.0 eq., 252 mg) was added, and the reaction mixture was stirred overnight. The solvent was removed under reduced pressure, and the crude product was purified by column chromatography (0–15% MeOH in DCM) to afford **I5** (192 mg, 89%) as a white solid. ^{1}H NMR (400 MHz, $CDCl_3$) δ 8.27 (dd, J = 6.4, 1.6 Hz, 2H), 7.36–7.30 (m, 4H), 7.30–7.17 (m, 10H), 6.97–6.85 (m, 4H), 4.09 (s, 4H), 3.19 (s, 4H). ^{13}C NMR (101 MHz, $CDCl_3$) δ 158.1, 140.3, 136.4, 130.9, 128.4, 127.6, 126.7, 118.0, 110.4, 71.4, 43.6, 37.5. HRMS-ESI: calcd for $C_{27}H_{26}N_2O_4$ $[M + H]^+$: 410.1895 found: 442.1893.

^{1}H NMR titration

^{1}H NMR titrations in CD_3CN were conducted at 298 K on a Varian Unity Inova 400 MHz system. Aliquots from a stock solution containing the corresponding salts were added sequentially to an NMR tube containing a solution of the ionophores (600 μL). The ^{1}H NMR spectrum was acquired after each addition. The ^{1}H NMR titration spectra were analyzed by MestReNova software. The NMR titration isotherms were fitted to a 1 : 1 host–guest binding model using Thordarson's equations[59,60] at **https://app.supramolecular.org/bindfit/**. The data were then plotted using OriginLab software. The binding constants K_a were presented with standard deviations from the fitting outcomes.

Isothermal titration calorimetry

Isothermal titration was performed on the MicroCal ITC_{200} system at 25 °C. The experiments were conducted in the 200 μL working volume of the sample cell. The capacity of the injection syringe is 40 μL. The stirring speed was set at 750 rpm. Host and guest solutions were prepared in MeCN. A host solution was placed in the titration cell, and the guests were loaded into the syringe. In each case, 20–25 injections were performed. The heat of dilution was measured by titrating the guest into a blank solution. The heat of dilution was subtracted before analyzing with MicroCal ITC_{200} software using a 1 : 1 host–guest binding model and plotted by Origin Lab software.

Computational modeling

Structural Optimization and Binding Energy Analysis: the Cartesian coordinates for the calculations were directly created using the GaussView 6 program. All optimizations were performed with density functional theory (DFT) in the Orca program[61] (version 4.2.1) using the Becke '88 exchange and Lee–Yang–Parr correlation (BLYP) functional,[62] the Ahlrich's double zeta Def2-SVP basis sets[63] with geometrical counterpoise (gCP) scheme,[64] and Grimme's third-generation dispersion correction[65] with Beck Johnson damping (D3BJ). In order to speed up the DFT optimizations, the Coulomb integral[66] and numerical chain-of-sphere integration[67] for the HF exchanges (RIJCOSX) method was applied with the Def2/J auxiliary basis (AuxJ).[68] All optimizations were performed in an acetonitrile continuum with the Conductor-like Polarizable Continuum Model (CPCM) in Orca. Multiwfn 3.6 program[69] was used to analyze the electrostatic potential map,[70] partial charges,[71] and noncovalent surfaces.[72,73]

Solid–liquid extraction

A solution of receptor **I5** (5 mM, 1 mL) in $CDCl_3$ was mounted on top of an excess amount of solid LiCl, NaCl and KCl, or a mixture of the three salts. The mixture was sonicated for 5 min. The resulting solution was pipetted into an NMR tube and measured by ^{1}H NMR spectroscopy. To release the captured LiCl, D_2O (1 mL) was added to the extractant, and the solution mixture was vortexed for 1 min, after which the organic phase was separated and measure by ^{1}H NMR.

Result and discussion

In pursuit of potential molecular scaffolds capable of binding Li^+ with strong affinity and high selectivity, we identified ionophore **I1**, initially reported[54] in 1986 for Li^+ sensing but with undetermined binding affinity and selectivity for ion binding. Intrigued by **I1**'s simple structure and unusual Li^+ selectivity, we opted to reexamine its binding properties. **I1** was synthesized following the original literature procedures. Its binding with Li^+ was initially assessed using ^{1}H NMR titrations in CD_3CN, employing $LiBF_4$ as a soluble salt. The binding affinity ($K_a > 10^6$ M^{-1}) between **I1** and Li^+ was found to be too high for reliable determination (Fig. S16 and S17†) by ^{1}H NMR titration at mM concentrations. We were only able to establish a 1 : 1 binding stoichiometry using this method. Alternatively, the binding constant ($K_a = 3.5 \times 10^6$ M^{-1}) was determined (Fig. 2) through isothermal titration calorimetry (ITC) experiments at a micromolar (70 μM) concentration. The binding affinity between **I1** and Na^+ is weak and can be determined by both ^{1}H NMR and ITC, which yielded a K_a in the order of 10^3 M^{-1}, resulting in a remarkable Li^+/Na^+ selectivity of 2214. This selectivity ranks among one of the highest reported[25,28,33,39,74–76] values for Li^+ receptors.

To provide a comparative assessment, we evaluated the binding affinities of two widely employed ionophores for Li^+ binding and capture, 12-crown-4 and dibenzo-14-crown-6. The 12-crown-4 exhibited a low binding affinity in the order of 10^3 M^{-1} for both Li^+ and Na^+. In fact, this macrocycle displays

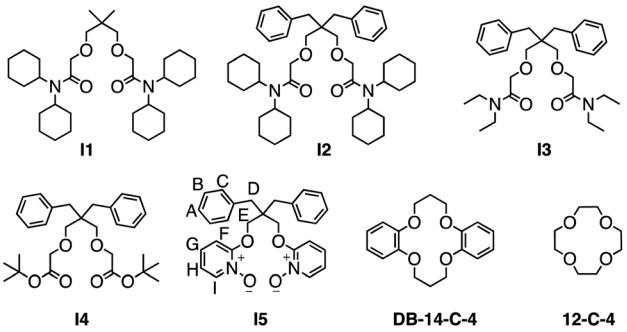

Fig. 1 Structural formula of the investigated Li^+ ionophores.

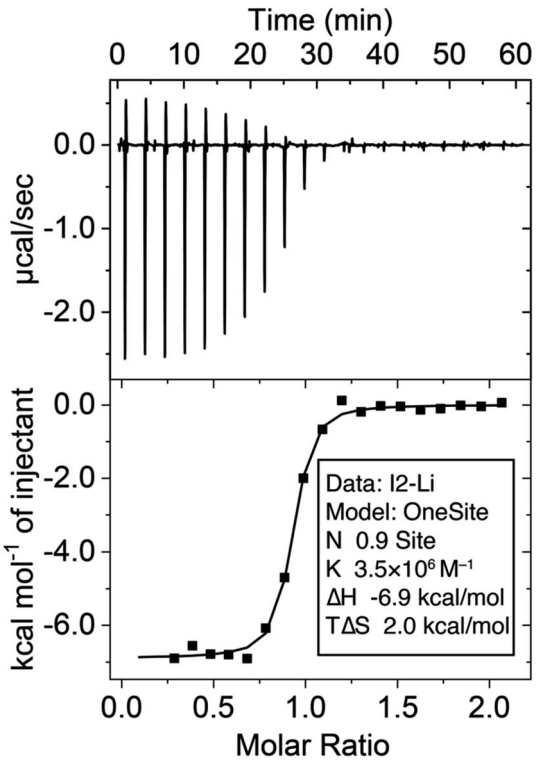

Fig. 2 Isothermal titration calorimetry of the binding between **I2** (0.1 mM in the cell) and $LiBF_4$ (1 mM in the syringe) in MeCN at 25 °C.

a slightly stronger affinity for Na^+ than Li^+, resulting in a Li^+/Na^+ selectivity of only 0.5. Consequently, the use of this macrocycle as a Li^+ ionophore is not recommended for selective Li^+ binding and capture.[77–80] In contrast, dibenzo-14-crown-4 demonstrated a higher Li^+ binding affinity in the order of 10^4 M^{-1} and a more favorable Li^+/Na^+ selectivity of 25, making it a popular choice for selective Li^+ binding. However, compared to **I1**, 12-crown-4 and dibenzo-14-crown-6 appear less attractive as ideal ionophores for Li^+ binding. Furthermore, the synthesis of **I1** is significantly simpler, as it does not involve a macrocyclization step, rendering **I1** a more practical option for serving as an ionophore for Li^+.

Motivated to elucidate the structural features responsible for the high affinity and selectivity for Li^+ associated with **I1**, we synthesized a library of its analogs, **I2–I5**. Initially, we incorporated two benzyl groups in **I2**, as evidence suggests[81] their potential to enhance Li^+ binding selectivity. ITC binding studies revealed that **I2** exhibited a binding affinity for Li^+ identical to that of **I1**. However, **I2** demonstrated a lower binding affinity for Na^+, resulting in an improved Li^+/Na^+ selectivity of 5645, which is over 200 times better than commonly used crown ether derivatives. ITC further indicated that the Li^+ binding of **I1** and **I2** is driven by favorable enthalpies, supported by a modest increase in entropy. The binding enthalpy of **I2** is slightly lower than that of **I1**, which is also evidenced by the less negative charges (Fig. S60 and S62†) associated with the oxygen atoms in **I2** compared to **I1**. This slight decrease in enthalpy is counterbalanced by a more favorable binding entropy due to the enhanced structural rigidity of **I2**.

A single crystal structure of **I2** (Fig. 3) was obtained *via* the slow evaporation of its solution in $CHCl_3$. The benzyl groups and *N*,*N*-dicyclohexylamide groups present in **I2** contribute to steric hindrances, restricting flexibility and supporting the hypothesis that the benzyl groups enhance the receptor **I2**'s rigidity for Li^+ binding. Our attempts to obtain a single crystal structure of **I2** in conjunction with Li^+ were unsuccessful. Instead, we derived an optimized structure (Fig. 3b) using density functional theory (DFT) calculations based on the reported crystal structure of the Li^+ complex with **I1**. Upon Li^+ binding, **I2** can reorganize its conformations to resemble the binding cavity of 14-crown-4, providing an ideal cavity size for Li^+. The Li^+ is positioned at the center of the binding cavity, stabilized by four [$Li^+\cdots O$] ion–dipole interactions. One of the benzyl groups is situated below the Li^+ ion. The electrostatic potential (ESP) map (Fig. 3c) indicates that the benzyl group generates a negatively charged surface area, potentially promoting Li^+ binding through favorable electrostatic attractions. The 14-crown-4-like binding cavity associated with **I1** and **I2** offers not only the appropriate size for Li^+ but also stronger ion–dipole interactions, rendering it superior for Li^+ binding.

I1 and **I2** exhibit a significantly lower binding affinity for Na^+ than Li^+. The primary reason is the larger ionic radius and, consequently, the lower charge density of Na^+, which results in weaker ion–dipole interactions. This diminished ion–dipole interaction with Na^+ is evidenced (Table 1 entries 2 and 4) by lower binding enthalpies. The presence of dibenzyl groups in **I2** further disfavors Na^+ binding by imposing an entropy penalty of -0.7 kcal mol^{-1}, suggesting a higher reorganization energy barrier required to accommodate the larger Na^+ ion within the 14-crown-4-like binding cavity.

Considering the clumsiness of *N*,*N*-dicyclohexyl substitutes, we aim to achieve better atomic efficiency for Li^+ capture using a smaller-sized ionophore **I3** with *N*,*N*-diethyl substituents. **I3** exhibited a comparable order of binding affinity and Li^+/Na^+ selectivity as **I1** and **I2**, though its overall performance decreased by a factor of two. **I3** displayed a stronger binding enthalpy in comparison to **I1** and **I2**. Owing to the smaller *N*,*N*-diethyl substituents, the size reduction increased **I3**'s structural flexibility, resulting in a less entropically favored Li^+ binding. The entropy–enthalpy compensation led to minimal changes in **I3**'s overall performance for Li^+ binding, suggesting that *N*,*N*-dicyclohexyl substituents are not essential for Li^+ binding. The binding between **I3** and Na^+ was slightly greater than that of **I2**, attributable to **I3**'s increased structural flexibility, which better accommodates Na^+. This interpretation is supported by a favorable entropy of 1.7 kcal mol^{-1} observed in ITC experiments.

Replacing the amide with esters in **I4** significantly diminished ion binding performance (Table 1, entries 7 and 8). The low affinities are because the carbonyl oxygen in esters is less electronegative than amide oxygen. Consequently, ester oxygen is a weaker electron donor for establishing ion–dipole interactions. As a result, **I4** demonstrated a significant decrease in binding enthalpy and affinity for Li^+ and Na^+.

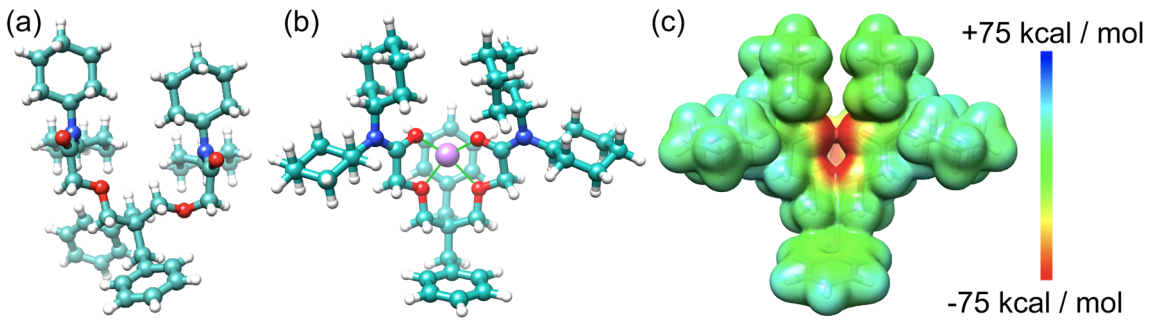

Fig. 3 (a) X-ray single crystal structure of **I2** and (b) an optimized structure of **I2** complexed with Li^+. (c) ESP of **I2** with reorganized conformation to fit the binding of Li^+.

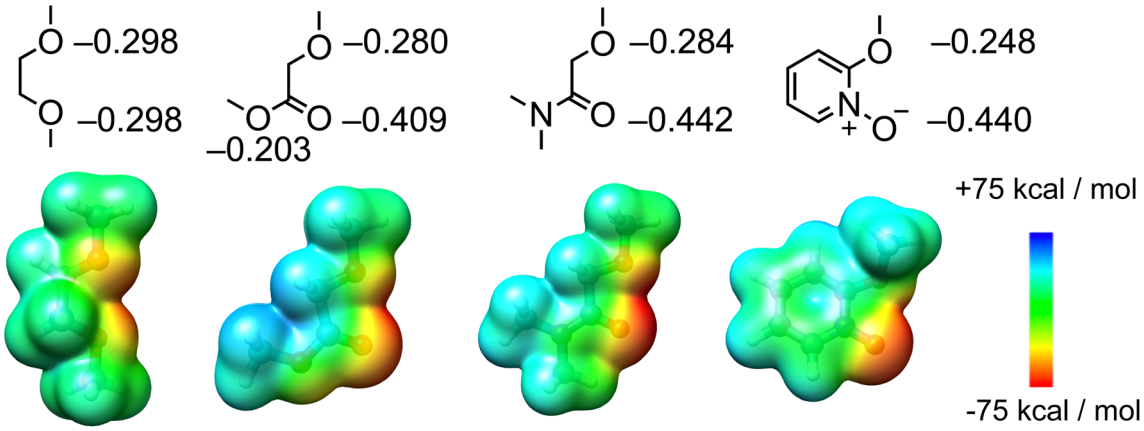

Fig. 4 Structural formula of the building blocks to construct Li^+ ionophores and calculated partial charges and ESP.

Table 1 Summary of binding thermodynamics parameters[a] determined by ^1H NMR and isothermal titration calorimetry

Entry	Complex	K_a (M^{-1}) NMR	ITC	ΔG (kcal mol^{-1})	ΔH (kcal mol^{-1})	$T\Delta S$ (kcal mol^{-1})	Li^+/Na^+ selectivity
1	**I1**-Li^+	$>10^6$	3.1×10^6	−8.6	−7.5	1.4	2214[d]
2	**I1**-Na^+	2.4×10^3	1.4×10^3	−4.3	−3.8	0.5	NA
3	**I2**-Li^+	$>10^6$	3.5×10^6	−8.9	−6.9	2.0	5645[d]
4	**I2**-Na^+	2.5×10^2	6.2×10^2	−3.8	−3.1	−0.7	NA
5	**I3**-Li^+	$>10^6$	1.4×10^6	−8.4	−8.2	0.18	1167[d]
6	**I3**-Na^+	2.9×10^2	1.2×10^3	−4.2	−2.5	1.7	NA
7	**I4**-Li^+	1.8×10^2	4.2×10^1	−2.2	−3.3	−1.1	NA
8	**I4**-Na^+	<5	NA[b]	NA	NA	NA	NA
9	**I5**-Li^+	1.2×10^5	8.0×10^4	−6.7	−5.5	1.2	1154[e]
10	**I5**-Na^+	1.0×10^2	NA[c]	NA[b]	NA[c]	NA[c]	NA
11	**DB-14-C-4**-Li^+	3.0×10^4	3.3×10^4	−6.2	−5.7	0.5	25[d]
12	**DB-14-C-4**-Na^+	6.1×10^2	1.3×10^3	−4.2	−2.4	1.8	NA
13	**12-C-4**-Li^+	2.5×10^3	3.5×10^3	−4.8	−1.2	3.6	0.5[d]
14	**12-C-4**-Na^+	1.4×10^4	6.4×10^3	−5.2	−7.0	−1.8	NA

[a] Standard errors are presented in the ESI. [b] The binding affinity to beyond the lower limit of ITC. [c] The low affinity and potential low binding enthalpy prevent ITC measurement. [d] The selectivity is based on ITC measurements. [e] The selectivity is based on NMR measurements.

By examining structural analogs of **I1**, we discovered that establishing strong ion–dipole interactions is crucial for achieving strong Li^+ binding affinity and high Li^+/Na^+ selectivity. To further validate this hypothesis, we designed receptor **I5** based on a new building block, pyridine-*N*-oxide, which exhibits a formal charge on the oxygen atom and should facilitate strong ion–dipole interactions. **I5** was designed with a binding pocket akin to that of 14-crown-4 and equipped with functionalities capable of establishing stronger ion–dipole interactions. **I5** can be readily synthesized (Fig. 5) from the diol precursor in two steps. A nucleophilic aromatic substitution reaction was employed to link two pyridine residues to the diol, followed by oxidation of the pyridine to pyridine-*N*-oxide, yielding the target ionophore **I5** in high efficiency.

The binding of **I5** with Li^+ was investigated through ^1H NMR titration experiments. Upon the addition of $LiBF_4$ to a solution of **I5** in CD_3CN, notable downfield shifts were observed for several proton signals (Fig. 6a). The most significant shifts originated from protons E, G, and I (proton labels depicted in Fig. 1), which are all in proximity to the binding pocket. The shifts ceased (Fig. 6c) after adding approximately one molar equivalent of $LiBF_4$, suggesting a 1 : 1 binding stoichiometry. By fitting the downfield shift of proton E, we determined (Fig. 6b) a binding affinity of 1.2×10^5 M^{-1} using a 1 : 1 binding model. The Li^+ binding by **I5** was independently corroborated by ITC, which exhibited a comparable binding constant in the order of 10^5 M^{-1}. ITC further revealed a high binding enthalpy (−5.5 kcal mol^{-1}) coupled with a favorable entropy (1.2 kcal-mol^{-1}). The high enthalpy can be ascribed to the anticipated strong ion–dipole interactions between the pyridine-*N*-oxide residues and Li^+, while the favorable entropy can be attributed to the relative rigidity of the molecular scaffold. The binding of **I5** with Na^+ was directly determined using ^1H NMR titrations, yielding a low K_a of 104 M^{-1}, which resulted in an outstanding Li^+/Na^+ selectivity of 1167. The experimental observation of strong Li^+ binding affinity and high Li^+/Na^+ selectivity facilitated by ion–dipole interactions was further corroborated by DFT calculations. Both amide and pyridine-*N*-oxide

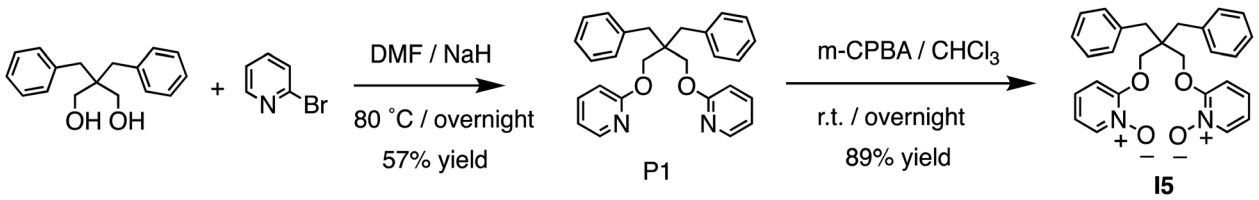

Fig. 5 Synthesis of new Li^+ ionophore **I5** based on pyridine-*N*-oxide.

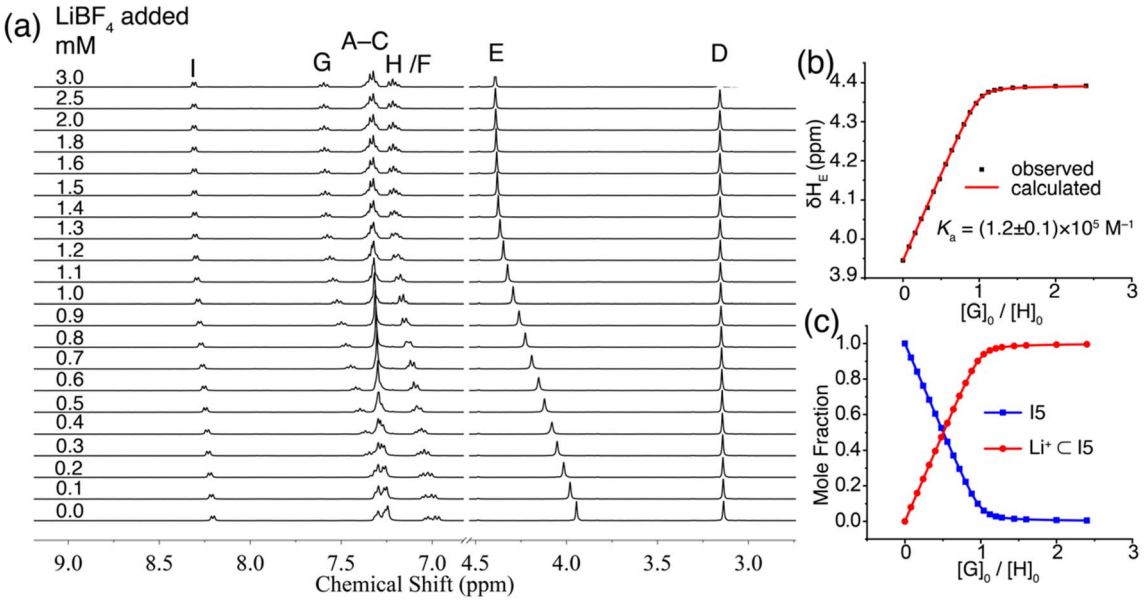

Fig. 6 (a) ^{1}H NMR (400 MHz, CD_3CN) spectrum of **I5** titrated with $LiBF_4$. (b) Nonlinear fitting for the chemical shift of proton E using a 1 : 1 binding model. (c) The molar ratio of **I5** and its Li^+ complex upon titrating $LiBF_4$.

demonstrated larger binding energies (Table S2†) and stronger noncovalent interactions (Fig. S60–S69†) in comparison to ester. These findings validate our hypothesis that potent ion–dipole interactions play a critical role in attaining substantial binding affinity and exceptional Li^+/Na^+ selectivity.

The binding affinity of **I5** for Li^+ is an order of magnitude lower than that of amide-based ionophores, such as **I1–I3**. ITC experiments suggest that this reduced binding affinity results from a lower binding enthalpy, indicating a weaker ion–dipole interaction for **I5**. This observation is further supported by the partial charges and ESP comparison (Fig. 4) between pyridine-*N*-oxide and etheryl amide building blocks. Although the pyridine-*N*-oxide oxygen exhibits a comparable electronegativity to the amide oxygen, the oxygen atom attached to the *ortho* position of the pyridine ring is less electronegative due to its conjugation with the aromatic ring. Consequently, the overall ion–dipole interaction associated with **I5** is weaker than that of the amide building block. However, considering the straightforward and cost-effective synthesis, coupled with its high binding affinity and Li^+/Na^+ selectivity, receptor **I5** represents an accessible ionophore for engineering Li^+ binding materials that outperform traditional crown ethers.

To demonstrate the potential application of ionophore **I5** in Li^+ separation, we conducted a solid–liquid extraction experiment. A solution of **I5** in $CDCl_3$ was placed atop an excess amount of LiCl or NaCl. The solution was sonicated for 5 minutes, and the extractant was monitored using ^{1}H NMR spectroscopy. The ^{1}H NMR spectrum of **I5** after NaCl extraction remained (Fig. 7) identical to that of the free **I5**, indicating no NaCl was extracted into the organic phase. In contrast, the ^{1}H NMR spectrum of **I5** after LiCl extraction displayed a distinct downfield shift of proton E, suggesting that **I5** can rapidly achieve complexation with LiCl and extracting it into the organic phase. This process involves the extraction of LiCl from its crystal lattice, overcoming the associated electrostatic attractions. Ion pair receptors, which possess a binding motif for cations and a binding motif for anions, are typically required for such solid–liquid extractions, and the process is generally slow, taking days to complete.[25,44] The high affinity and selectivity of **I5** enable rapid extraction of LiCl into the organic phase within 5 minutes, demonstrating its exceptional performance in Li^+ extraction. The extracted Li^+ can be easily released from the organic phase to an aqueous solution by a simple wash with D_2O, after which the ^{1}H NMR spectrum of **I5** resumes (Fig. 7a) back to its uncomplex state. We performed (Fig. 7b) four cycles of LiCl extraction followed by its release into D_2O without observing a significant loss of its extraction capacity.

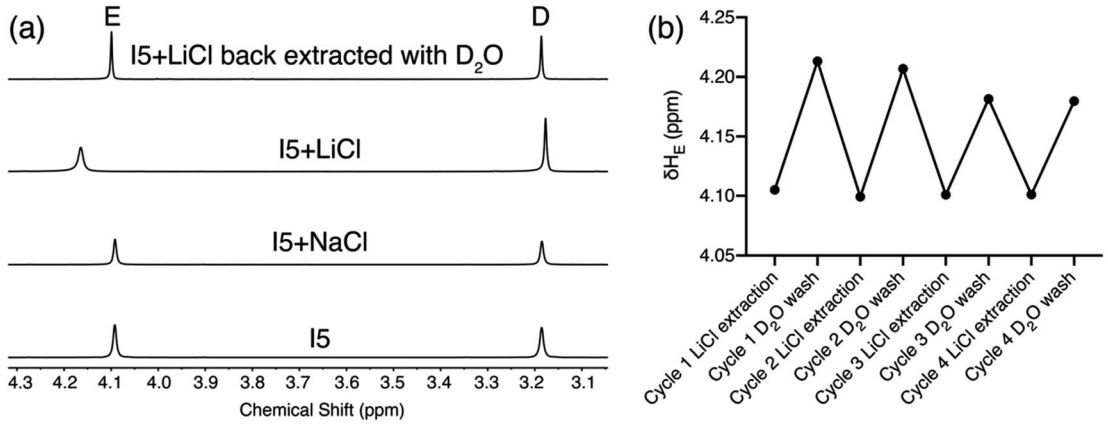

Fig. 7 (a) ^{1}H NMR (400 MHz, $CDCl_3$) spectra of **I5** to track the solid–liquid extraction of LiCl and NaCl. (b) Changes in the chemical shift of proton E during four cycles of LiCl extraction using $CDCl_3$ and release in D_2O using **I5**.

To further demonstrate the applicability of receptor **I5** for Li^+ separation, we conducted a solid–liquid extraction experiment from a sample containing only 0.2% LiCl in the presence of a significant excess of NaCl and KCl, two common salts that coexist in large excess in real-world scenarios. The ^{1}H NMR spectrum of **I5** after extraction (see Fig. S70 and S71†) showed the same chemical shift as the one saturated with LiCl, suggesting the high Li^+ selectivity associated with **I5**.

Conclusion

In summary, we have demonstrated the binding of Li^+ using five ionophores and compared their performances with traditional Li^+ receptors based on crown ethers. These ionophores demonstrated a much better binding affinity and Li^+/Na^+ selectivity when associated with functional groups that show strong ion–dipole interactions. In addition, a new building block based on pyridine-*N*-oxide was identified as an effective motif for the design of receptors to bind Li^+. We also demonstrated a rapid and efficient process for solid–liquid extraction of LiCl in the presence of large access of NaCl and KCl to organic solvent using ionophore **I5**. Overall, these studies are expected to advance our understanding of molecular design strategies for producing high-performance receptors targeted for the recognition and extraction of the critical mineral lithium. These receptors are expected to facilitate lithium extraction and separation when grafted onto a polymeric backbone as an immobilized extraction agent. We are currently exploring other molecular skeletons integrated with strong ion–dipole interactions to achieve better affinities and selectivities for Li^+.

Author contributions

C. X. and Q. T. performed the experiments. L. W. solved the crystal structure. W. L. and C. X. designed the experiment, analyzed the results, and wrote the manuscript. All authors discussed the results and revised the manuscript.

Conflicts of interest

There are no conflicts to declare.

Acknowledgements

Financial support for this work was provided by the University of South Florida start-up funding. This work was supported, in part, by the University of South Florida Research & Innovation Internal Awards Program under Grant No. 0154360. This research made use of the X-RAY and CPAS Core facilities at the University of South Florida. The research was supported in part by the computational resources provided by the CIRCE research cluster facility at the University of South Florida.

Notes and references

1 S. K. Sarai, H. M. Mekala and S. Lippmann, *Innov. Clin. Neurosci.*, 2018, **15**, 30–32.
2 Z. M. Kamal, S. Dutta, S. Rahman, A. Etando, E. Hasan, S. N. Nahar, W. F. S. Wan Ahmad Fakuradzi, S. Sinha, M. Haque and R. Ahmad, *Cureus*, 2022, **14**, e29332.
3 C. Venkateswaran, H. Sreemoolanadhan and R. Vaish, *Int. Mater. Rev.*, 2022, **67**, 620–657.
4 N. Kumar, V. Saini and J. Bijwe, *Tribol. Lett.*, 2020, **68**, 124.
5 S. Yang, F. Zhang, H. Ding, P. He and H. Zhou, *Joule*, 2018, **2**, 1648–1651.
6 E. A. Olivetti, G. Ceder, G. G. Gaustad and X. Fu, *Joule*, 2017, **1**, 229–243.
7 X. Sun, M. Ouyang and H. Hao, *Joule*, 2022, **6**, 1738–1742.
8 M. Armand and J.-M. Tarascon, *Nature*, 2008, **451**, 652–657.
9 S. Kim, H. Joo, T. Moon, S. H. Kim and J. Yoon, *Environ. Sci.: Processes Impacts*, 2019, **21**, 667–676.
10 C. Liu, Y. Li, D. Lin, P.-C. Hsu, B. Liu, G. Yan, T. Wu, Y. Cui and S. Chu, *Joule*, 2020, **4**, 1459–1469.
11 Z. Li, C. Li, X. Liu, L. Cao, P. Li, R. Wei, X. Li, D. Guo, K. W. Huang and Z. Lai, *Energy Environ. Sci.*, 2021, **14**, 3152–3159.

12 A. Alessia, B. Alessandro, V. G. Maria, V. A. Carlos and B. Francesca, *J. Cleaner Prod.*, 2021, **300**, 126954.
13 X. Luo, B. Guo, J. Luo, F. Deng, S. Zhang, S. Luo and J. Crittenden, *ACS Sustainable Chem. Eng.*, 2015, **3**, 460–467.
14 P. Xu, J. Hong, X. Qian, Z. Xu, H. Xia, X. Tao, Z. Xu and Q. Q. Ni, *J. Mater. Sci.*, 2021, **56**, 16–63.
15 J. F. Song, L. D. Nghiem, X. M. Li and T. He, *Environ. Sci.: Water Res. Technol.*, 2017, **3**, 593–597.
16 K. I. Hong, H. Kim, Y. Kim, M. G. Choi and W. D. Jang, *Chem. Commun.*, 2020, **56**, 10541–10544.
17 S. Tsuchiya, Y. Nakatani, R. Ibrahim and S. Ogawa, *J. Am. Chem. Soc.*, 2002, **124**, 4936–4937.
18 H. Piotrowski, K. Polborn, G. Hilt and K. Severin, *J. Am. Chem. Soc.*, 2001, **123**, 2699–2700.
19 Z. Grote, M. L. Lehaire, R. Scopelliti and K. Severin, *J. Am. Chem. Soc.*, 2003, **125**, 13638–13639.
20 Q. He, Z. Zhang, J. T. Brewster, V. M. Lynch, S. K. Kim and J. L. Sessler, *J. Am. Chem. Soc.*, 2016, **138**, 9779–9782.
21 H. Gohil, S. Chatterjee, S. Yadav, E. Suresh and A. R. Paital, *Inorg. Chem.*, 2019, **58**, 7209–7219.
22 X. Guo, Y. Yang, Z. Peng, Y. Cai, W. Feng and L. Yuan, *Org. Chem. Front.*, 2019, **6**, 2654–2661.
23 K. Severin, *Coord. Chem. Rev.*, 2003, **245**, 3–10.
24 Q. He, G. I. Vargas-Zúñiga, S. H. Kim, S. K. Kim and J. L. Sessler, *Chem. Rev.*, 2019, **119**, 9753–9835.
25 Q. He, N. J. Williams, J. H. Oh, V. M. Lynch, S. K. Kim, B. A. Moyer and J. L. Sessler, *Angew. Chem., Int. Ed.*, 2018, **57**, 11924–11928.
26 V. K. Munasinghe, J. Pancholi, D. Manawadu, Z. Zhang and P. D. Beer, *Chem.–Eur. J.*, 2022, **28**, 1–8.
27 Y. Luo, N. Marets and T. Kato, *Chem. Sci.*, 2018, **9**, 608–616.
28 M. Kamenica, R. Kothur, A. Willows, B. Patel and P. Cragg, *Sensors*, 2017, **17**, 2430.
29 Z. Grote, R. Scopelliti and K. Severin, *J. Am. Chem. Soc.*, 2004, **126**, 16959–16972.
30 Z. Chen, O. F. Schall, M. Alcalá, Y. Li, G. W. Gokel and L. Echegoyen, *J. Am. Chem. Soc.*, 1992, **114**, 444–451.
31 D. J. Cram, T. Kaneda, G. M. Lein and R. C. Helgeson, *J. Chem. Soc., Chem. Commun.*, 1979, **21**, 948–950.
32 D. J. Cram, S. P. Ho, C. B. Knobler, E. Maverick and K. N. Trueblood, *J. Am. Chem. Soc.*, 1986, **108**, 2989–2998.
33 D. J. Cram and G. M. Lein, *J. Am. Chem. Soc.*, 1985, **107**, 3657–3668.
34 P. A. Kollman, G. Wipff and U. C. Singh, *J. Am. Chem. Soc.*, 1985, **107**, 2212–2219.
35 D. J. Cram, T. Kaneda, R. C. Helgeson, S. B. Brown, C. B. Knobler, E. Maverick and K. N. Trueblood, *J. Am. Chem. Soc.*, 1985, **107**, 3645–3657.
36 D. J. Cram and I. B. Dicker, *J. Chem. Soc., Chem. Commun.*, 1982, 1219–1221.
37 O. Shyshov, R. C. Brachvogel, T. Bachmann, R. Srikantharajah, D. Segets, F. Hampel, R. Puchta and M. von Delius, *Angew. Chem., Int. Ed.*, 2017, **56**, 776–781.
38 R. C. Brachvogel, F. Hampel and M. Von Delius, *Nat. Commun.*, 2015, **6**, 1–7.
39 H. Löw, E. Mena-Osteritz and M. Von Delius, *Chem. Sci.*, 2018, **9**, 4785–4793.
40 S. Kitazawa, K. Kimura, H. Yano and T. Shono, *J. Am. Chem. Soc.*, 1984, **106**, 6978–6983.
41 B. P. Czech, D. A. Babb, B. Son and R. A. Bartsch, *J. Org. Chem.*, 1984, **49**, 4805–4810.
42 I. Oral and V. Abetz, *Macromol. Rapid Commun.*, 2021, **42**, 2000746.
43 K. Kobiro, *Coord. Chem. Rev.*, 1996, **148**, 135–149.
44 J. M. Mahoney, A. M. Beatty and B. D. Smith, *Inorg. Chem.*, 2004, **43**, 7617–7621.
45 H. Wang, L. O. Jones, I. Hwang, M. J. Allen, D. Tao, V. M. Lynch, B. D. Freeman, N. M. Khashab, G. C. Schatz, Z. A. Page and J. L. Sessler, *J. Am. Chem. Soc.*, 2021, **143**, 20403–20410.
46 Q. He, N. J. Williams, J. H. Oh, V. M. Lynch, S. K. Kim, B. A. Moyer and J. L. Sessler, *Angew. Chem., Int. Ed.*, 2018, **57**, 11924–11928.
47 Q. He, Z. Zhang, J. T. Brewster, V. M. Lynch, S. K. Kim and J. L. Sessler, *J. Am. Chem. Soc.*, 2016, **138**, 9779–9782.
48 C. Ren, V. Maurizot, H. Zhao, J. Shen, F. Zhou, W. Q. Ong, Z. Du, K. Zhang, H. Su and H. Zeng, *J. Am. Chem. Soc.*, 2011, **133**, 13930–13933.
49 M. Sheikh, M. Qassem, I. F. Triantis and P. A. Kyriacou, *Sensors*, 2022, **22**, 736.
50 S. I. Pascu, T. Jarrosson, C. Naumann, S. Otto, G. Kaiser and J. K. M. Sanders, *New J. Chem.*, 2005, **29**, 80–89.
51 G. Kaiser, T. Jarrosson, S. Otto, Y. F. Ng, A. D. Bond and J. K. M. Sanders, *Angew. Chem., Int. Ed.*, 2004, **43**, 1959–1962.
52 X. Ruan, C. Zhang, Y. Zhu, F. Cai, Y. Yang, J. Feng, X. Ma, Y. Zheng, H. Li, Y. Yuan and G. Zhu, *Angew. Chem., Int. Ed.*, 2023, **62**, e202216549.
53 M. L. Lehaire, R. Scopelliti, H. Piotrowski and K. Severin, *Angew. Chem., Int. Ed.*, 2002, **41**, 1419–1422.
54 E. Metzger, R. Aeschimann, M. Egli, G. Suter, R. Dohner, D. Ammann, M. Dobler and W. Simon, *Helv. Chim. Acta*, 1986, **69**, 1821–1828.
55 M. Bocheńska and M. Gdaniec, *J. Incl. Phenom. Mol. Recognit. Chem.*, 1994, **20**, 53–71.
56 A. R. De Sànchez, J. R. Anacona and V. E. Màrquez, *Supramol. Chem.*, 1994, **4**, 9–12.
57 J. V. Gavette, J. Lara, L. L. Reling, M. M. Haley and D. W. Johnson, *Chem. Sci.*, 2013, **4**, 585–590.
58 U. Olsher, R. M. Izatt, J. S. Bradshaw and N. K. Dalley, *Chem. Rev.*, 1991, **91**, 137–164.
59 D. Brynn Hibbert and P. Thordarson, *Chem. Commun.*, 2016, **52**, 12792–12805.
60 P. Thordarson, *Chem. Soc. Rev.*, 2011, **40**, 1305–1323.
61 F. Neese, *Wiley Interdiscip. Rev.: Comput. Mol. Sci.*, 2012, **2**, 73–78.
62 A. D. Becke, *J. Chem. Phys.*, 1993, **98**, 5648–5652.
63 F. Weigend and R. Ahlrichs, *Phys. Chem. Chem. Phys.*, 2005, **7**, 3297–3305.
64 H. Kruse and S. Grimme, *J. Chem. Phys.*, 2012, **136**, 154101.
65 S. Grimme, J. Antony, S. Ehrlich and H. Krieg, *J. Chem. Phys.*, 2010, **132**, 154104.
66 F. Weigend, *Phys. Chem. Chem. Phys.*, 2006, **8**, 1057–1065.
67 R. Izsák and F. Neese, *J. Chem. Phys.*, 2011, **135**, 144105.

68 G. L. Stoychev, A. A. Auer and F. Neese, *J. Chem. Theory Comput.*, 2017, **13**, 554–562.
69 T. Lu and F. Chen, *J. Comput. Chem.*, 2012, **33**, 580–592.
70 J. Zhang and T. Lu, *Phys. Chem. Chem. Phys.*, 2021, **23**, 20323–20328.
71 T. LU and F. CHEN, *J. Theor. Comput. Chem.*, 2012, **11**, 163–183.
72 T. Lu and Q. Chen, *J. Comput. Chem.*, 2022, **43**, 539–555.
73 C. Lefebvre, G. Rubez, H. Khartabil, J. C. Boisson, J. Contreras-García and E. Hénon, *Phys. Chem. Chem. Phys.*, 2017, **19**, 17928–17936.
74 J. M. Lehn and J. P. Sauvage, *J. Am. Chem. Soc.*, 1975, **97**, 6700–6707.
75 D. J. Cram, T. Kaneda, R. C. Helgeson, S. B. Brown, C. B. Knobler, E. Maverick and K. N. Trueblood, *J. Am. Chem. Soc.*, 1985, **107**, 3645–3657.
76 K. Roy, C. Wang, M. D. Smith, P. J. Pellechia and L. S. Shimizu, *J. Org. Chem.*, 2010, **75**, 5453–5460.
77 S. J. Warnock, R. Sujanani, E. S. Zofchak, S. Zhao, T. J. Dilenschneider, K. G. Hanson, S. Mukherjee, V. Ganesan, B. D. Freeman, M. M. Abu-Omar and C. M. Bates, *Proc. Natl. Acad. Sci.*, 2021, **118**, e2022197118.
78 S. D. Alexandratos and C. L. Stine, *React. Funct. Polym.*, 2004, **60**, 3–16.
79 P. K. Mohapatra, D. S. Lakshmi, A. Bhattacharyya and V. K. Manchanda, *J. Hazard. Mater.*, 2009, **169**, 472–479.
80 M. Kazemabad, A. Verliefde, E. R. Cornelissen and A. D'Haese, *J. Membr. Sci.*, 2020, **595**, 117432.
81 K. Kimura, H. Yano, S. Kitazawa and T. Shono, *J. Chem. Soc., Perkin Trans. 2*, 1986, **4**, 1945–1951.